JCB Journal of Cell Biology

ARTICLE

Prolonged cyclin-dependent kinase inhibition results in septin perturbations during return to growth and mitosis

Gabriel M. Gihana, Tiffany R. Musser, Oscar Thompson, and Soni Lacefield

We investigated how *Saccharomyces cerevisiae* coordinate polarization, budding, and anaphase during a unique developmental program called return to growth (RTG) in which cells in meiosis return to mitosis upon nutrient shift. Cells reentering mitosis from prophase I deviate from the normal cell cycle by budding in G2 instead of G1. We found that cells do not maintain the bipolar budding pattern, a characteristic of diploid cells. Furthermore, strict temporal regulation of M-phase cyclin-dependent kinase (CDK; M-CDK) is important for polarity establishment and morphogenesis. Cells with premature M-CDK activity caused by loss of checkpoint kinase Swe1 failed to polarize and underwent anaphase without budding. Mutants with increased Swe1-dependent M-CDK inhibition showed additional or more penetrant phenotypes in RTG than mitosis, including elongated buds, multiple buds, spindle mispositioning, and septin perturbation. Surprisingly, the enhanced and additional phenotypes were not exclusive to RTG but also occurred with prolonged Swe1-dependent CDK inhibition in mitosis. Our analysis reveals that prolonged activation of the Swe1-dependent checkpoint can be detrimental instead of beneficial.

Introduction

Progression through the cell cycle is controlled by a complex regulatory system that ensures the temporal order of events. Cyclin-dependent kinases (CDKs) bound to cyclins are major drivers of the cell cycle. The order of events is maintained by the recognition of specific substrates by cyclin-bound CDK and by the quantitative increase in CDK activity as the cell cycle progresses (Enserink and Kolodner, 2010; Uhlmann et al., 2011). Each cell cycle stage is coupled to changes in cell morphogenesis to ultimately allow proper partitioning of the genome between two daughter cells. Although there is evidence that CDK either directly or indirectly regulates cell morphogenesis, how cell cycle events coordinate with changes in cell morphogenesis is poorly understood.

Budding yeast is an excellent model organism to study the link between cell cycle and cell morphogenesis. During vegetative growth, budding yeast cells polarize the cytoskeleton and organize membrane growth to form a bud, which becomes the daughter cell. The morphogenetic steps of bud emergence and growth are cell cycle regulated and CDK dependent. A single CDK, Cdc28, functions with nine cyclins to govern the cell cycle (Enserink and Kolodner, 2010). In G1, polarity establishment and bud formation require the activity of Cdc28 bound to G1 cyclins. Polarity is established through local recruitment of the conserved Rho family GTPase Cdc42, which specifies the site of bud emergence (Adams et al., 1990; Johnson and Pringle, 1990; Ziman et al., 1993; Richman et al., 2002). The site of Cdc42 polarization is not random. Instead, Cdc42 accumulates at sites designated by spatial cues inherited from the previous division cycle (Howell and Lew, 2012). Growth is targeted to the bud tip (apical growth) from late G1 through S phase. In G2, Cdc28 binds M-phase cyclins (M-CDKs) and initiates the apical–isotropic switch, and growth occurs uniformly throughout the bud cortex (Farkas et al., 1974; Lew and Reed, 1993). Bud length depends on the duration of apical growth (Lew and Reed, 1993). A delay in the apical–isotropic switch prolongs growth at the bud tip, causing elongated buds. In contrast, a premature apical–isotropic switch leads to abnormally spherical buds.

The G2/M transition and the onset of anaphase is regulated by the highly conserved CDK-inhibitory kinase *Saccharomyces cerevisiae* Wee1 (Swe1) homologue and the phosphatase Mih1 (Cdc25 homologue) that removes the inhibitory phosphate (Gould and Nurse, 1989; Russell et al., 1989; Gould et al., 1990; Booher et al., 1993; Lianga et al., 2013). Swe1 and Mih1 have only minor roles in an unperturbed cell cycle. *swe1Δ*

Department of Biology, Indiana University, Bloomington, IN.

Correspondence to Soni Lacefield: sonil@indiana.edu.

https://doi.org/10.1083/jcb.201708153

cells are somewhat reduced in cell size, whereas *mih1Δ* cells are increased in cell size (Russell et al., 1989; Jorgensen et al., 2002; Harvey and Kellogg, 2003; Pal et al., 2008). However, both Swe1 and Mih1 have a central role in the morphogenesis checkpoint, which delays cells at G2 in response to conditions that cause osmotic stress, actin perturbation, septin defects, and disruptions of membrane growth (Lew and Reed, 1995; Sia et al., 1996, 1998; McMillan et al., 1998; Barral et al., 1999; Alexander et al., 2001; McNulty and Lew, 2005; Anastasia et al., 2012). In the presence of these perturbations, regulation of both Swe1 and Mih1 activity results in CDK inhibition and a delay before the isotropic switch (Sia et al., 1998; Pal et al., 2008; Wicky et al., 2011; Anastasia et al., 2012). In an unperturbed cell cycle, Swe1 protein abundance is periodic, peaking at S/G2 (McMillan et al., 1998; Sia et al., 1998). The protein is hyperphosphorylated and targeted for degradation at the septin collar at the end of G2 (Kaiser et al., 1998; Sia et al., 1998; Shulewitz et al., 1999; Sreenivasan and Kellogg, 1999; Cid et al., 2001; McMillan et al., 2002; Harvey et al., 2005). Perturbations that prevent budding or that affect septin organization can result in prolonged Swe1 activity (Barral et al., 1999; Shulewitz et al., 1999; Longtine et al., 2000; Cid et al., 2001; McMillan et al., 2002; Theesfeld et al., 2003; Kang et al., 2016). Once cells have budded, assembled a septin collar, and inactivated Swe1, the inhibitory phosphorylation on M-CDK is reversed by the Mih1, Ptp1, and possibly PP2A phosphatases, allowing mitosis initiation (Russell et al., 1989; Harvey and Kellogg, 2003; Pal et al., 2008; Kennedy et al., 2016).

In this study, we address the question of how cells coordinate cell cycle events with changes in morphogenesis in a unique developmental program in budding yeast called return to growth (RTG), in which cells exit meiosis and resume mitosis if shifted to nutrient-rich medium before the meiotic commitment point (Ganesan et al., 1958; Sherman and Roman, 1963; Simchen et al., 1972; Esposito and Esposito, 1974; Honigberg and Esposito, 1994; Zenvirth et al., 1997; Friedlander et al., 2006; Nachman et al., 2007; Dayani et al., 2011; Tsuchiya et al., 2014). The switch from meiotic prophase I to mitosis is a particularly intriguing cell cycle transition. Cells bud in G2 rather than G1 as they do in normal mitosis. In addition, cells at the end of prophase I have replicated DNA and undergone meiosis-specific events such as the initiation of recombination, pairing of homologous chromosomes, and assembly of synaptonemal complex (Fig. 1 A; Winter, 2012). Remarkably, upon nutrient-rich medium addition, cells disassemble the synaptonemal complex, repair recombination intermediates, bud, and then undergo a mitotic division (Dayani et al., 2011; Winter, 2012; Tsuchiya and Lacefield, 2013). Hence, cells undergoing RTG bud in G2 after DNA replication, reversing the normal order of events that occur during mitosis. We investigated how cell cycle regulation is modulated to coordinate polarity establishment, bud formation, and timely nuclear division during RTG. We find an important role in regulating Swe1 activity during RTG to properly coordinate polarized growth with cell cycle events. Furthermore, our results establish that prolonged activation of the morphogenesis checkpoint in both RTG and normal mitosis can be detrimental.

Results

Bud site selection is random during RTG

During normal mitosis in budding yeast, the location of the bud site does not occur at random. Instead, cells inherit cortical landmark proteins that determine the site of Cdc42 recruitment. Once accumulated and activated, Cdc42 catalyzes downstream events for bud formation (Bi and Park, 2012). Diploid budding yeast cells bud in a bipolar pattern in which mother cells bud either adjacent to or opposite from the previous division site; daughter cells bud opposite from the division site (Fig. 1 B; Freifelder, 1960; Chant and Pringle, 1995; Harkins et al., 2001). Whether bud site selection spatial cues are maintained in meiosis and used in RTG for a bipolar budding pattern is not known.

We compared the pattern of bud site selection in RTG and mitosis by staining cells with calcofluor, which binds chitin in the cell wall and marks birth and bud scars from the previous division site (Pringle, 1991). We grew cells in medium with calcofluor and used time-lapse microscopy to detect the new bud site with respect to the scar. To observe RTG, we allowed cells to reach prophase I and then added nutrient-rich medium with calcofluor and observed the first bud. Cells had a deletion of *NDT80*, which encodes a transcription factor needed to exit prophase I; thus, these cells were arrested in prophase I at the time of nutrient addition (Xu et al., 1995; Winter, 2012). Fig. 1 (C and D) shows calcofluor-stained cells in RTG and mitosis, respectively, both before (left) and after (right) budding. We analyzed cells with only one scar to definitively identify the previous division site. We measured the central angle between the previous division site and nascent bud. Cells in RTG did not bud with a bipolar pattern but instead budded with a somewhat random distribution (Fig. 1 E). In contrast and as expected from previous work, most mitotic cells budded either adjacent to or opposite from the previous division site, with a larger fraction of cells budding at the opposite pole (Chant and Pringle, 1995; Harkins et al., 2001). These results demonstrate that during RTG, cells do not maintain the bipolar budding pattern.

A failure to maintain bipolar budding could occur during meiosis or during the starvation conditions used to initiate meiosis. To differentiate between these possibilities, we analyzed bud pattern in cells with a deletion of *IME1*, a gene required for meiosis initiation. *ime1Δ* cells were treated with the same starvation conditions used for our RTG analysis. Upon nutrient addition, we found that *ime1Δ* cells did not bud at random but tended to bud toward the opposite pole (Fig. S1 A). However, the trend was not as strong as mitotic cells. This is similar to findings from a previous study that showed that starvation and refeeding of diploid cells only somewhat disrupted bipolar budding (Chant and Pringle, 1995). Therefore, our results suggest that spatial cues that direct bipolar budding in mitosis are not maintained in meiosis.

Polarization, bud formation, and anaphase are delayed during RTG

The first step of polarity establishment is the local accumulation of GTP-bound Cdc42 (GTP-Cdc42), which recruits septins, actin, and cell wall material for bud formation (Howell and Lew,

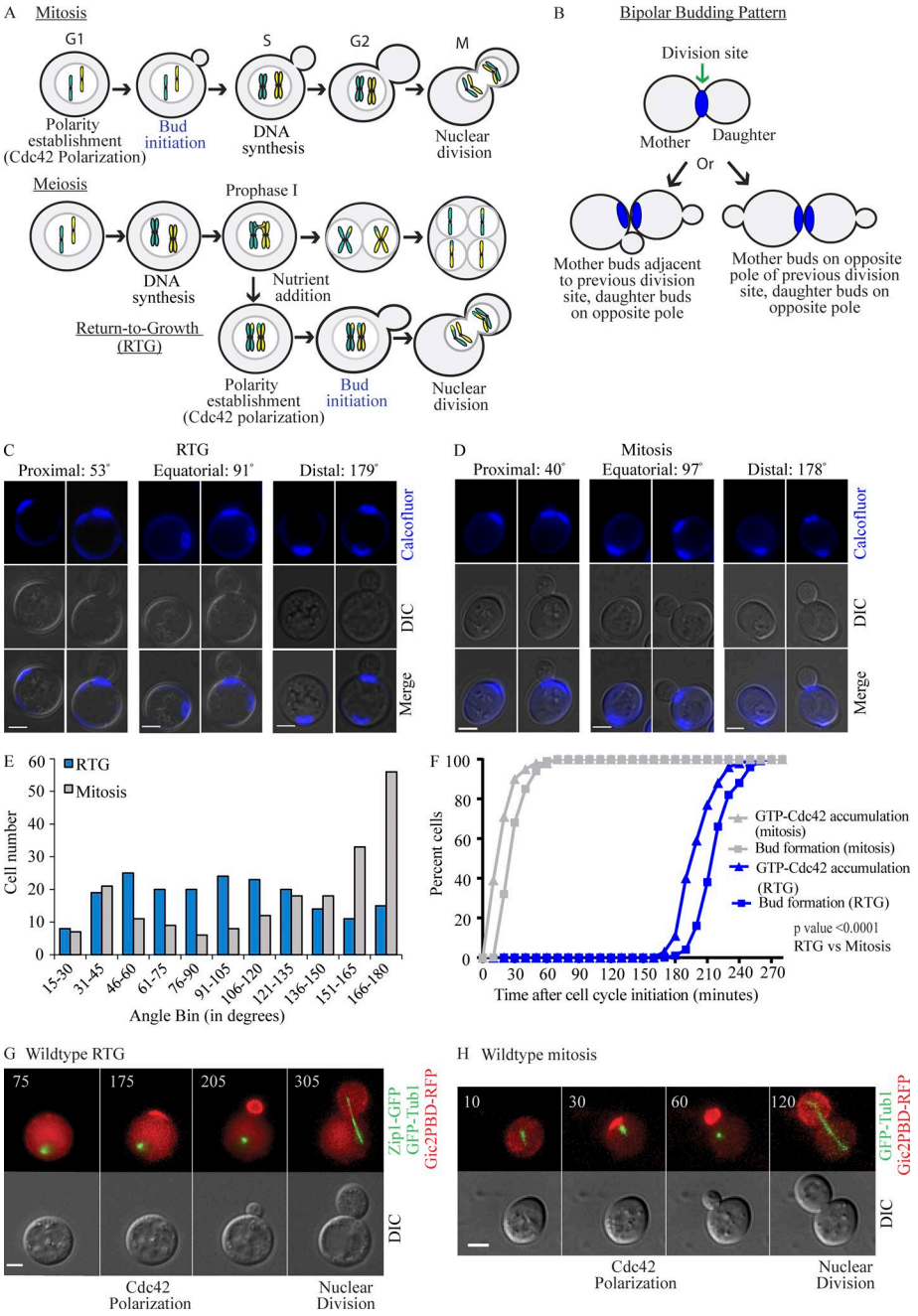

Figure 1. **Budding pattern, polarity establishment, and bud formation during RTG. (A)** Cartoon of mitosis, meiosis, and RTG. **(B)** Cartoon of bipolar budding pattern in diploid cells with calcofluor (blue) at the division site. **(C and D)** Time-lapse images of calcofluor-stained cells during RTG and mitosis, respectively. The same cell is shown before (left) and after (right) budding with angle between the bud scar and new bud. **(E)** Absolute frequency of budding angles in RTG and mitosis (n = 200 cells each). **(F)** Time of GTP-Cdc42 accumulation and bud formation during RTG and mitosis. For RTG, time was measured from nutrient addition (n = 100 cells). For mitosis, time was measured from anaphase spindle breakdown (n = 100 cells). Differences between RTG and mitosis for time of GTP-Cdc42 accumulation and bud formation are statistically significant (Mann-Whitney test with computation of exact two-tailed p-value; P < 0.0001). **(G and H)** Time-course images of GTP-Cdc42 accumulation in a WT cell undergoing RTG and mitosis, respectively. Time in minutes is indicated. DIC, differential interference contrast. Bars, 3 µm.

2012). We analyzed the polarization time of Cdc42 during RTG and mitosis by monitoring cells expressing Gic2-PBD-RFP (the Gic2 p21 binding domain fused to RFP), which acts as a GTP-Cdc42 biosensor because it specifically binds GTP-bound Cdc42 (Gulli et al., 2000; Okada et al., 2013). The cells also expressed two proteins tagged with GFP: Zip1, a component of the synaptonemal complex, and Tub1, α-tubulin. Monitoring Zip1-GFP allowed us to detect cells in prophase I because the synaptonemal complex assembles and disassembles in prophase I (White et al., 2004; Scherthan et al., 2007). Monitoring GFP-Tub1 allowed us to determine the time of anaphase onset based on spindle elongation (Straight et al., 1997; Tsuchiya et al., 2011). Both proteins were tagged with GFP, but they were distinguishable because they were morphologically and temporally distinct.

During RTG, cells budded 223 ± 20 min (mean ± SD) after nutrient-rich medium production (Fig. 1, F and G). In mitosis, cells budded 29 ± 10 min after the previous division. In both RTG and mitosis, cells polarized GTP-Cdc42 10–20 min before budding (Fig. 1, F and H). The longer duration for polarization and budding during RTG could be explained by the requirement for cells to first exit meiosis and then acquire the proteins needed for local accumulation and activation of Cdc42.

After budding, anaphase onset was also slower in RTG when compared with mitosis. During RTG, anaphase onset occurred 315 ± 29 min after nutrient-rich medium introduction, which was 90 min after budding (Table S1). In mitosis, cells underwent anaphase 93 ± 16 min after spindle breakdown from the previous anaphase, which was 64 min after budding. Thus, the time

from budding to anaphase onset was 30 min longer in RTG than in mitosis. This result was unexpected. In RTG, cells do not rereplicate their DNA after budding, whereas in mitosis, cells undergo DNA replication after budding. Therefore, we expected a faster anaphase onset in RTG compared with mitosis.

A genetic screen identifies genes required for coordination of polarity, bud growth, and nuclear division during RTG

The long duration of polarity establishment and anaphase onset during RTG suggested a difference in the coordination of cell cycle regulation and bud growth. We performed a genome-scale screen with the yeast knockout collection (Tong et al., 2001) to identify mutants that either underwent anaphase without budding or that had prolonged apical bud growth during RTG. We hypothesized that mutants unable to link bud morphogenesis with cell division may undergo nuclear division without budding and become binucleate. Mutants that fail to efficiently organize their cytoskeleton may prolong apical bud growth in response to the morphogenesis checkpoint and delay cells before the apical–isotropic switch, creating long-budded cells (Howell and Lew, 2012). We used a series of mating, sporulation, and selection to obtain diploids homozygous for each knockout, for *ndt80Δ*, and for Zip1-GFP (detailed screen design in Fig. S1 B). To perform the screen, mutant cells were induced to enter meiosis and arrest at prophase I; nutrient-rich medium was then added to allow cells to return to mitosis and initiate budding (Fig. 2 A). The cells were then fixed, stained with DAPI, and imaged to identify mutants that were either binucleate (more than one DAPI spot) or long budded. After the primary screen, we verified the results with a knockout in our strain background. We also performed time-lapse imaging of normal mitosis and only further investigated mutants that gave unique or enhanced phenotypes in RTG compared with normal mitosis.

The screen identified nine genes that, for ease of discussion, we are calling polarized growth regulators (PGRs). Eight PGR mutants formed long buds during RTG: *mih1Δ*, *clb2Δ*, *hsl7Δ*, *hsl1Δ*, *gin4Δ*, *nap1Δ*, *elm1Δ*, and *cla4Δ*. In addition to long buds, *gin4Δ* and *elm1Δ* also had binucleate cells. One PGR, *swe1Δ*, was isolated as a binucleate mutant but with a distinct phenotype from *gin4Δ* and *elm1Δ* in that *swe1Δ* cells failed to bud but underwent nuclear division during RTG, in agreement with our previous work (Tsuchiya and Lacefield, 2013). Unlike *swe1Δ* cells, *gin4Δ* and *elm1Δ* cells budded but frequently failed to properly divide their nuclei into mother and daughter cells because of spindle positioning defects (see description below).

All the mutants identified in the screen lack proteins that either directly or indirectly regulate CDK activity. Swe1 phosphorylates and inhibits M-CDK during the morphogenesis checkpoint to delay cells at G2 (Booher et al., 1993; Sia et al., 1996). Mih1 removes the inhibitory phosphate to reactivate M-CDK (Russell et al., 1989; Harvey and Kellogg, 2003). Clb2 is the major B-type cyclin that activates M-CDK (Surana et al., 1991). Hsl7, Hsl1, and Elm1 are needed for recruitment of Swe1 to the septin collar for subsequent degradation. In the absence of these proteins, there is an increase in active Swe1 (Barral et al., 1999; Shulewitz et al., 1999; Longtine et al., 2000; Cid et al., 2001; Kang et al., 2016). Gin4, Nap1, Cla4, and Elm1 regulate septin organization (Longtine et al., 1998a, 2000; Sreenivasan and Kellogg, 1999; Bouquin et al., 2000; Weiss et al., 2000; Gladfelter et al., 2004, 2005; Versele and Thorner, 2004; Asano et al., 2006). Previous work showed that defects in septin organization cause a Swe1-dependent delay, resulting in prolonged inhibition of M-CDK (Barral et al., 1999). Although the mutants only caused mild phenotypes during normal mitosis, the phenotypes were exacerbated during RTG, possibly because of increased M-CDK activity (*swe1Δ*) or decreased M-CDK activity (*mih1Δ*, *clb2Δ*, *hsl7Δ*, *hsl1Δ*, *gin4Δ*, *nap1Δ*, *elm1Δ*, and *cla4Δ*).

swe1Δ cells fail to polarize during RTG

The only mutant isolated from our screen that failed to bud and became binucleate during RTG was *swe1Δ*, with 95–98% of cells becoming binucleate as previously shown (Fig. 2 B; Tsuchiya and Lacefield, 2013). Fig. 2 B shows the consequence of a binucleate division with the mother cell acquiring an extra nucleus in the next mitotic division after RTG. Because *swe1Δ* cells did not bud, we analyzed whether they could establish GTP-Cdc42 polarity. Using time-lapse microscopy, we monitored GTP-Cdc42 localization with the Gic2-PBD-RFP biosensor. We found that *swe1Δ* cells did not polarize GTP-Cdc42 before nuclear division during RTG but did polarize GTP-Cdc42 during the next mitotic cell cycle after RTG (Fig. 2, B and C). In mitosis, *swe1Δ* cells polarized GTP-Cdc42 with similar timing as WT cells (Figs. 1 F and 2, C and D). The *mih1Δ* cells polarized GTP-Cdc42 with the same timing as WT cells during RTG (Figs. 1 F and 2, E and F). However, *mih1Δ* cells showed extensive GTP-Cdc42 accumulation at the bud tips as well as a prolonged delay in the time of anaphase onset when compared with WT cells (Fig. 2 E and Table S1). In mitosis, *mih1Δ* cells polarized GTP-Cdc42, budded, and underwent anaphase with similar timing as WT cells (Figs. 1 H and 2, F and G). Overall, these results suggest that RTG requires a more precise temporal regulation of M-CDK activity than mitosis by Swe1 and Mih1. During RTG, the inhibition of M-CDK activity by Swe1 is essential for polarity establishment and budding and to prevent binucleate cells. The timely relief from M-CDK inhibition by Mih1 is also essential to ensure correct timing of anaphase and normal Cdc42 GTPase activity at the bud tip.

PGR mutants have an exacerbated long-bud phenotype and enhanced M-CDK inhibition during RTG

Like *mih1Δ*, the other mutants isolated from our screen had elongated buds during RTG (Fig. 3 A). Some of the mutants were previously reported to have long-budded cells in a subset of the population during vegetative growth (Fig. 3 B; Surana et al., 1991; Blacketer et al., 1993; Cvrcková et al., 1995; Kellogg and Murray, 1995; Ma et al., 1996; Altman and Kellogg, 1997). Thus, we quantified the percentage of long-budded cells in RTG and in mitosis. We also determined the timing of bud formation and anaphase onset in RTG and mitosis (Fig. 3, C and D). As shown in Fig. 3 C, all mutants budded with similar timing as WT cells in both RTG and mitosis. In contrast, the mutants had a delayed anaphase onset compared with WT cells in RTG (Fig. 3 D and Table S1). Notably, the *cla4Δ* mutant cells were exceptional as they failed to divide for the duration of the video (10 h after nutrient addition). This phenotype was rare during mitosis.

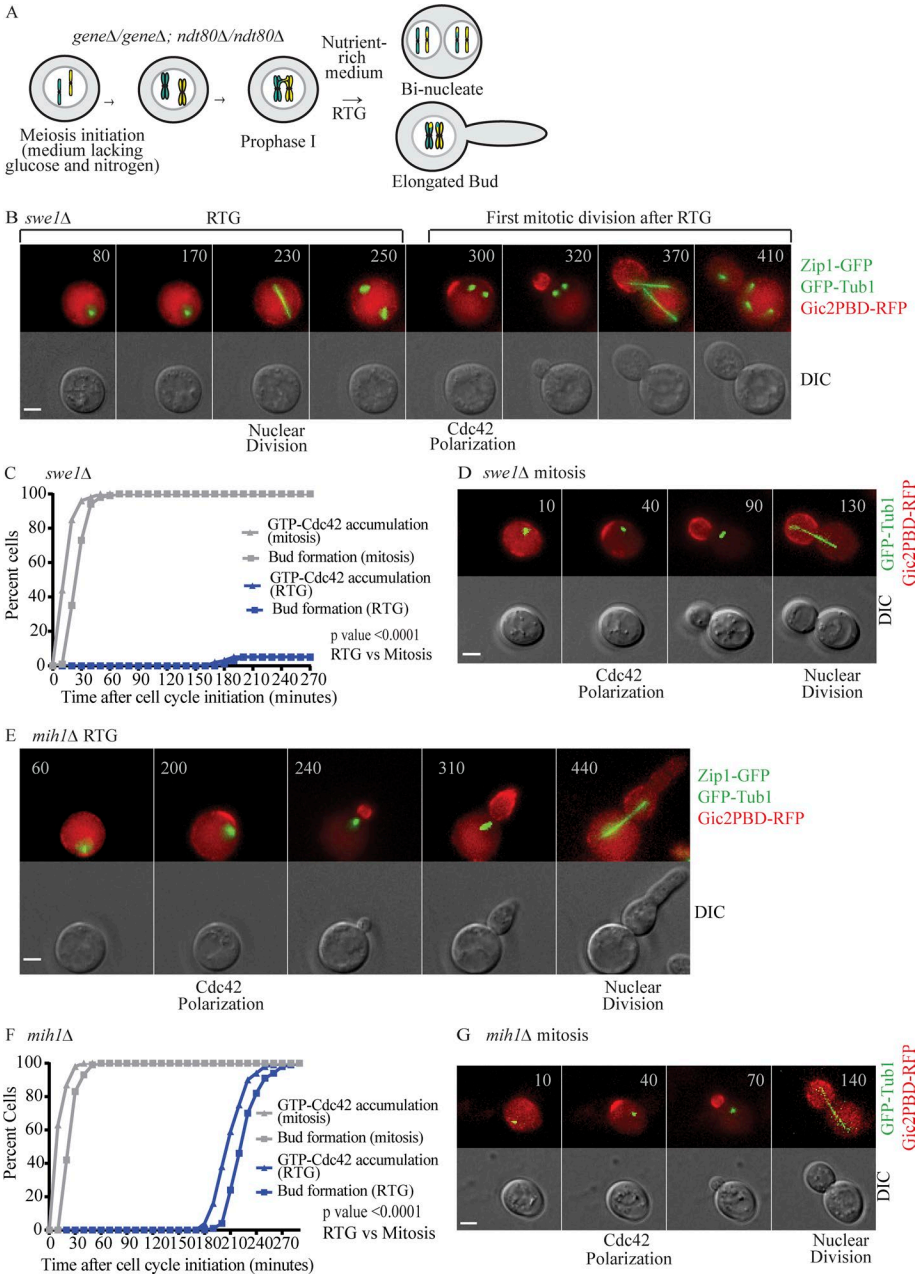

Figure 2. **A genetic screen isolated mutants in which polarity and cell growth are uncoordinated with nuclear division. (A)** A simplified screen outline. **(B–G)** Time in minutes after nutrient-rich medium addition (RTG) or after the previous spindle breakdown (mitosis). **(B)** Time-lapse images of a *swe1Δ* cell during RTG that fails to polarize GTP-Ccd42 or bud yet undergoes a nuclear division. **(C)** Time of GTP-Cdc42 accumulation and budding in *swe1Δ* cells during RTG and mitosis are statistically significantly different (Mann-Whitney test with computation of two-tailed exact p-value; $P < 0.0001$; $n = 100$ cells each). **(D)** Time-lapse images of a *swe1Δ* cell during mitosis with GTP-Cdc42 accumulation, budding, and anaphase. **(E)** Time-lapse images of a *mih1Δ* cell during RTG with an elongated bud and hyperpolarized GTP-Cdc42 at the bud tip. **(F)** Time of GTP-Cdc42 accumulation and budding during RTG and mitosis in *mih1Δ* cells ($n = 100$ cells each). Differences are statistically significant (Mann-Whitney test with computation of two-tailed exact p-value; $P < 0.0001$). **(G)** Time-lapse images of a *mih1Δ* cell showing GTP-Cdc42 accumulation, budding, and nuclear division during mitosis. DIC, differential interference contrast. Bars, 3 µm.

Next, we measured the bud length at anaphase onset in all mutants except *cla4Δ*, which was measured after 450 min. Each mutant had an increased mean bud length during RTG when compared with WT cells (Fig. 3 E). Also, the mean bud length for all the mutants except *elmΔ* was greater in RTG compared with mitosis. In *elm1Δ*, the mean bud length was similar in mitosis and RTG. We counted the percentage of cells with elongated buds during RTG and mitosis, defining an elongated bud as greater than two SDs from the mean bud length of WT cells. Most of the PGR mutants undergoing RTG had long buds ($n = 100$; Fig. 3 F). In mitosis, all mutants except *elm1Δ* had a smaller proportion of long-budded cells (Fig. 3, E and F). *mih1Δ* and *clb2Δ* cells did not have elongated buds in mitosis. These results demonstrate that except for *elm1Δ*, the long-bud phenotype of the PGR mutants was exacerbated and more penetrant during RTG than during mitosis.

Analysis of the long-budded cells in RTG showed that some mutants budded more than once from the mother cell before division, a rare phenotype in mitosis (Fig. 4 A and Video 1). The *hsl1Δ*, *gin4Δ*, *nap1Δ*, and *cla4Δ* mutants reached metaphase (based on spindle length) but then established a new site of polarity and formed another bud before completing cell division. This intriguing behavior suggests a profound loss of coupling between morphogenesis and cell cycle regulation ($n = 200$; Fig. 4 B).

The formation of long-budded cells suggests a delayed apical–isotropic switch with prolonged growth directed toward the bud tip. Because Swe1 activity could block this switch by inhibitory phosphorylation of M-CDK, we analyzed each mutant for CDK phosphorylation. We isolated protein at time points after RTG induction and performed Western blots with an antibody against Y19-phosphorylated CDK, the

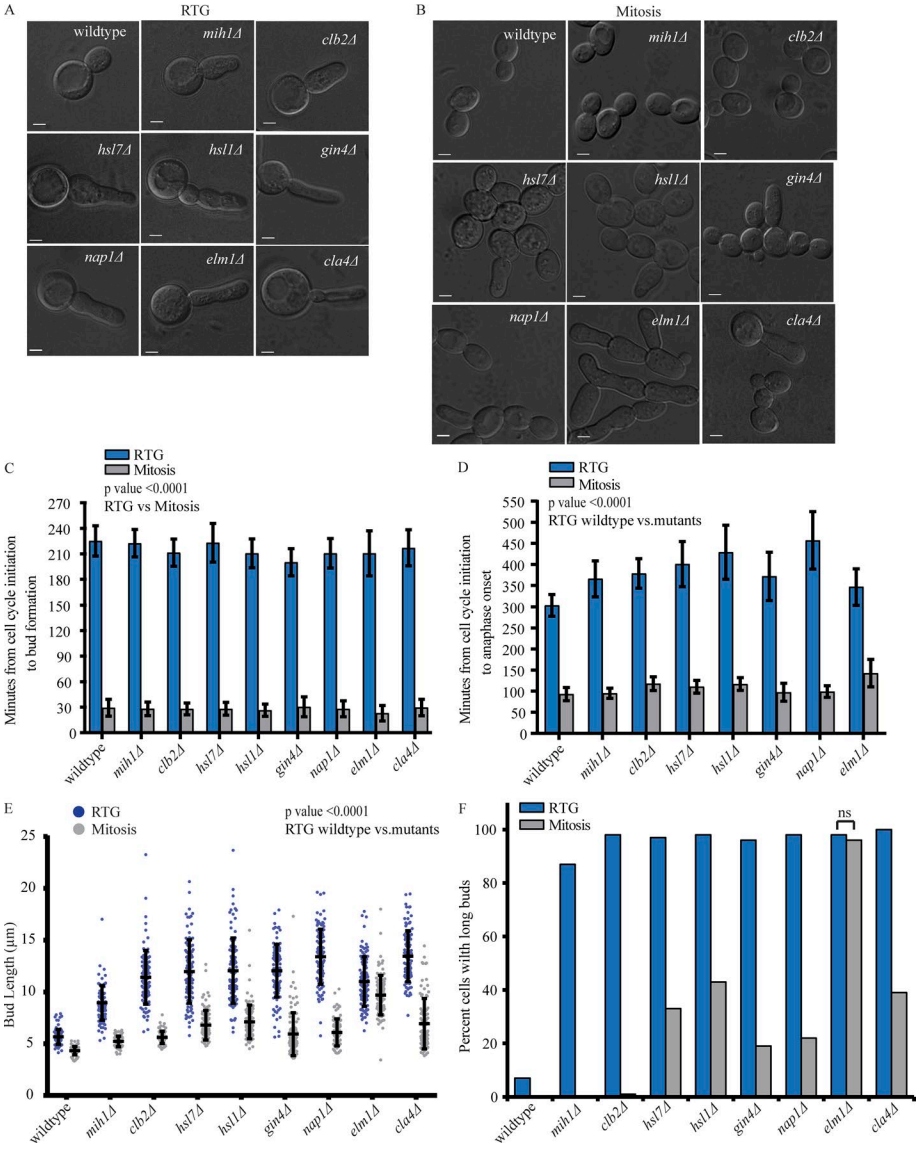

Figure 3. **The PGRs are dispensable during mitosis but crucial during RTG. (A and B)** Images of WT and elongated bud mutants during RTG (A) and during mitosis (B). Bars, 3 µm. **(C and D)** Mean time of bud formation and anaphase during RTG and mitosis (n = 100 each). For RTG, time in minutes measured from transfer to nutrient-rich medium to bud formation (C) or anaphase onset (D). For mitosis, time in minutes measured from previous spindle breakdown. **(E)** Mean bud length during both RTG and mitosis (n = 100 for each). Differences between WT and each mutant during RTG are statistically significant for time of anaphase onset and bud length (Mann-Whitney test with computation of two-tailed exact p-value; $P < 0.001$). **(F)** Percentage of cells with elongated buds during RTG and during mitosis (n = 100 each). Differences were statistically significant (Two-tailed Fisher's exact test; $P < 0.05$) unless marked ns. Error bars indicate SD.

phosphorylation Swe1 specifically puts on CDK. WT cells had peak CDK phosphorylation at 120 min after nutrient addition and then decreased levels (Figs. 4 C and S2 A). As expected, *swe1Δ* cells did not show Y19-phosphorylated CDK. PGR mutants had a greater extent of phosphorylated CDK than WT cells especially at 270 and 300 min, a time by which mutants are delayed in metaphase while WT cells are entering anaphase (Fig. S2 B). These results suggest that during RTG, PGR mutants have enhanced Swe1 inhibition of M-CDK, which delays cells in M phase and causes elongated buds. In addition, the results demonstrate that during RTG, M-CDK inhibition by Swe1 starts before bud formation, which does not occur in mitosis (Harvey and Kellogg, 2003; Harvey et al., 2005; Pal et al., 2008; Lianga et al., 2013). We hypothesize that because Swe1 is active and required for budding during RTG, minor perturbations that increase Swe1 activity could lead to more penetrant and more pronounced defects during RTG than during normal mitosis. Together, these data suggest that a strict temporal regulation of M-CDK activity is essential for normal morphogenesis during RTG.

Some of the PGR mutants have spindle positioning defects during RTG

Time-lapse imaging of *hsl1Δ*, *gin4Δ*, *nap1Δ*, *elm1Δ*, and *cla4Δ* mutant cells revealed an increased percentage of cells with spindle positioning defects during RTG compared with mitosis (Fig. 5 A). In WT cells, the spindle elongated across the bud neck (Fig. 5 B). In the mutants, we found several examples of aberrant spindle positioning: (A) the spindle prematurely migrated into the bud and then elongated back into the mother (Fig. 5 C); (B) the spindle first elongated in the mother and then crossed the bud neck (Fig. 5, D and E); and (C) the spindle elongated and broke down in the mother, creating a binucleate mother (Fig. 5 F). The *hsl1Δ*, *gin4Δ*, *nap1Δ*, and *elm1Δ* mutants had the largest fraction of cells with mispositioned spindles during RTG. For example, *elm1Δ* cells mispositioned spindles in ~30% of mitotic divisions, but this number increased to 75% of RTG divisions, with 56% of cells dividing the nucleus within the mother. Fig. S3 shows the percentage of cells in each class. These data suggest that PGRs ensure proper nuclear migration and genomic stability during RTG.

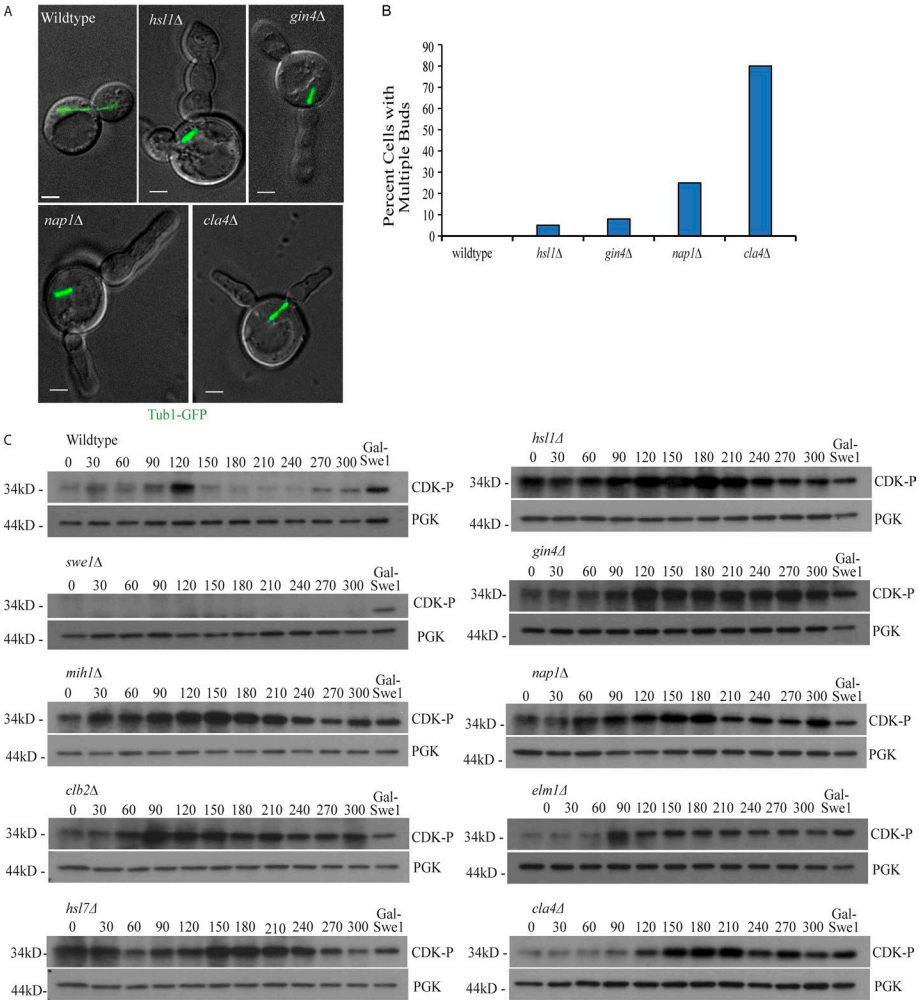

Figure 4. **During RTG, some PGR mutants bud multiple times, and all mutants have enhanced Tyr19-phosphorylated CDK. (A)** Images from a time-lapse experiment showing formation of two buds before nuclear division in *hsl1Δ*, *gin4Δ*, *nap1Δ*, and *cla4Δ* cells during RTG. Bars, 3 µm. **(B)** Percentage of cells that budded multiple times before nuclear division during RTG (n = 200 each). **(C)** Western blots with anti–Tyr19-phosphorylated CDK (CDK-P) and anti-PGK antibodies. PGK served as a loading control. Numbers indicate time points in minutes after transfer to nutrient-rich medium from meiotic prophase I. A sample from cells overexpressing Swe1 for 300 min in mitosis served as a reference standard for CDK phosphorylation.

The PGR mutants have septin defects during RTG

Gin4, Nap1, Elm1, and Cla4 are involved in septin organization and the mutants to have some septin defects in vegetative cells (Longtine et al., 1998a, 2000; Sreenivasan and Kellogg, 1999; Bouquin et al., 2000; Weiss et al., 2000; Gladfelter et al., 2004, 2005; Versele and Thorner, 2004; Asano et al., 2006). Because previous work has shown that a G2/M delay can exacerbate minor septin defects (Gladfelter et al., 2005), we analyzed whether the mutants had enhanced septin defects during RTG. Our analysis also included the *mih1Δ*, *clb2Δ*, *hsl7Δ*, and *hsl1Δ* mutants. We integrated a construct with *CDC3-GFP*, a GFP-tagged component of the septins in a haploid strain at the *LEU2* locus (Okada et al., 2013). We then mated the haploid to a strain without the Cdc3-GFP construct; the strain therefore had one copy of *CDC3-GFP* and two copies of the endogenous *CDC3*. Time-lapse microscopy confirmed that WT cells with the *CDC3-GFP* construct underwent RTG and mitosis with normal timing and with a single septin collar at the bud neck (Fig. 6, A and B). The septin collar split into two rings after the cells underwent nuclear division in both RTG and mitosis. A striking difference between the mutants and WT cells is that there were additional septin structures in the buds of all mutants before nuclear division during RTG. In fact, most of *hsl1Δ*, *gin4Δ*, *nap1Δ*, *elm1Δ*, and *cla4Δ* cells had additional structures (Fig. 6, C and D; and Video 2). Only the *elm1Δ* cells had a high percentage of additional septin structures during mitosis as previously shown (Sreenivasan and Kellogg, 1999). The most surprising observation was that the *mih1Δ*, *clb2Δ*, and *hsl7Δ* mutants also had additional septin structures. These mutants are not known to have a role in regulating septin organization.

The time-lapse imaging with a deconvolution microscope suggested that some mutants had defective bud-neck septin collars. To better resolve septin structures, we analyzed each mutant with superresolution imaging and counted the percentage of cells with defective bud-neck septin structures in both RTG and mitosis (Fig. 6, E and F). All septin structures in WT cells appeared normal during RTG and mitosis. In contrast, PGR mutants displayed a range of defects including disorganized, abnormally shaped, and abnormally sized septin collars (Fig. 6 E). *elm1Δ* and *cla4Δ* mutants had a high percentage of cells with defective septin bud-neck structures in both RTG and mitosis. The *clb2Δ*, *hsl1Δ*, *gin4Δ*, and *nap1Δ* mutants had a significantly higher fraction of cells with defective structures during RTG (Fig. 6 F). The results from our septin analyses suggest that all mutants except *elm1Δ* had enhanced septin defects, including additional septin structures in the buds and perturbed bud-neck septin structures during RTG compared with mitosis.

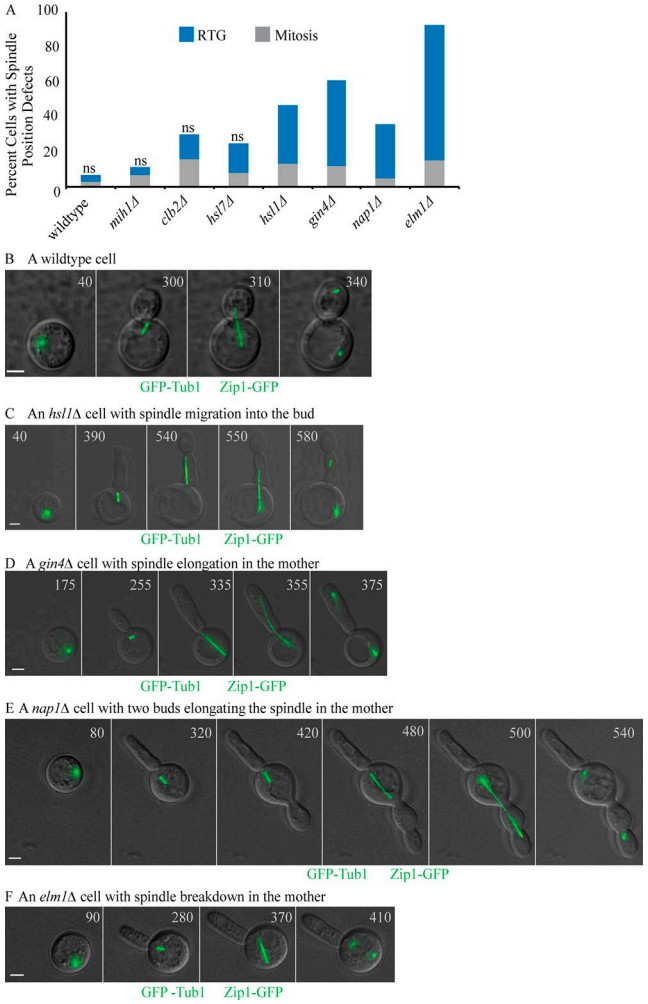

Figure 5. **Aberrant spindle positioning in PGR mutants. (A)** Percentage of cells with aberrant spindle positioning during RTG and mitosis (n = 200 each). Differences between RTG and mitosis are statistically significantly (Two-tailed Fisher's exact test; P < 0.001) unless marked ns. **(B–F)** Time-lapse images showing aberrant spindle positions during RTG with time in minutes after nutrient-rich medium addition. Bars, 3 µm.

Swe1 overexpression causes elongated buds, multiple buds, spindle positioning defects, and septin disorganization during mitosis

A feature common among the mutants was that they all showed enhanced inhibitory phosphorylation of CDK by Swe1 and also had enhanced septin defects during RTG (Figs. 4 C and 6, D and F). Therefore, we hypothesized that the prolonged G2/M delay is sufficient to cause septin defects. We also hypothesized that this phenotype was not exclusive to RTG but was revealed in RTG as a result of enhanced Swe1 activity. We tested our hypothesis by asking whether overexpressing Swe1 in otherwise WT mitotic cells would yield the same phenotypes observed with the PGR mutants during RTG.

To overexpress *SWE1*, we replaced both copies of the *SWE1* promoter in diploid cells with the *GAL1* promoter and grew cells in galactose-containing medium. The cells grew normally in raffinose-containing medium, which has low P_{GAL1}-*Swe1* expression. In microfluidic chambers, we grew cells in raffinose-containing medium and then flowed in galactose-containing medium as time-lapse imaging was performed. Cells also expressed *CDC3-GFP* to monitor septin and *mCherry-TUB1* to monitor the spindle. We overexpressed Swe1 for 360 min, a time range in which some PGR mutants are initiating anaphase during RTG (Table S1). In cells overexpressing *SWE1*, we observed all phenotypes that we described for the mutants during RTG. First, as expected from previous work, cells with *SWE1* overexpression had elongated buds when compared with cells grown in raffinose, with a mean bud length of 22 ± 6 µm (mean ± SD) compared with 4 ± 1 µm in cells without *SWE1* overexpression (measured at anaphase onset; Fig. 7, A–D; and Videos 3 and 4; Booher et al., 1993; Lim et al., 1996; Gladfelter et al., 2005). Second, after 360 min of *SWE1* overexpression, 37% of cells had formed a second bud (Fig. 7, B and E; and Video 5). Third, the cells showed defective spindle positioning, with the spindle migrating into the bud in 97% of cells after 300 min of *SWE1* overexpression (Fig. 7, A, B, and E; and Videos 3 and 5). None of the cells completed anaphase during the duration of the imaging (420 min). Fourth, additional septin structures formed at constrictions within the elongating buds (Fig. 7, A, B, and E). Fifth, superresolution microscopy revealed that 43% of cells had defective septin structures at the bud neck after 360 min of *SWE1* overexpression but had normal septin structures at bud formation. Only 2% of cells showed defective bud neck septin structures when *SWE1* was not overexpressed (Fig. 7, F and G). Additionally, the septin structures at the bud neck seemed to become dimmer over time during time-lapse imaging. To further quantitate this result without the possibility of photobleaching, we took individual time points at bud formation and at the metaphase delay (210 min later) and measured mean fluorescence intensity of bud neck septins. The bud neck septin structures became less intense over time when Swe1 was overexpressed (Fig. 7 H). To determine whether this phenotype also occurs in PGR mutants during RTG, we measured the intensity of bud neck septin structures in *hsl1Δ* and *nap1Δ* mutants at bud formation and metaphase delay (210 min later), and we observed a decrease in septin intensity. Superresolution imaging showed that *hsl1Δ* and *nap1Δ* mutants also did not have defective bud neck septin structures at bud formation but acquired defects during the metaphase delay (Fig. 1 G). These results suggest that M-CDK activity is required to maintain the original septin structure at the bud neck during the cell cycle.

Finally, we examined GTP-Cdc42 polarization at the bud tip in cells overexpressing Swe1. In normal mitosis, GTP-Cdc42 polarizes at one cortical site and recruits septins and actin to form a bud (Ziman et al., 1993; Richman et al., 2002; Howell and Lew, 2012; Okada et al., 2013). We hypothesized that with *SWE1* overexpression, GTP-Cdc42 could recruit septins to the bud tip. We monitored Gic2-PBD-RFP (GTP-Cdc42 biosensor) and Cdc3-GFP localization over time. We also monitored spindle position and cell cycle progression with mCherry-Tub1. After prolonged bud tip accumulation of GTP-Cdc42, Cdc3-GFP also appeared colocalized with GTP-Cdc42; a constriction formed, and Cdc3-GFP remained at the constriction while the bud tip elongated with GTP-Cdc42 at the tip. Several cycles of GTP-Cdc42 polarization and septin recruitment continued, forming an elongated bud with septin at the constrictions (Fig. 7 I and Video 6).

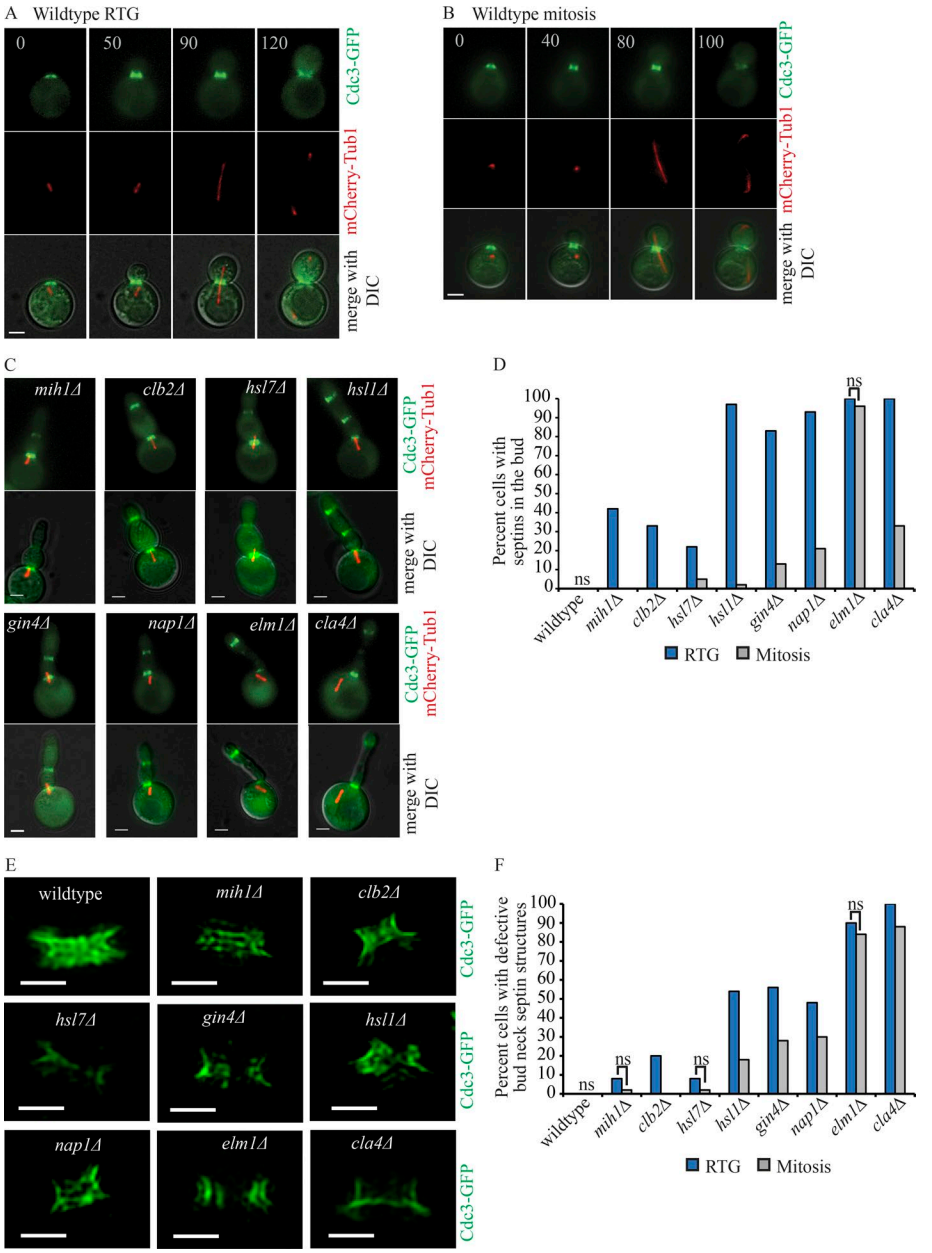

Figure 6. **Abnormal septin localization and organization in PGR mutants during RTG. (A–C)** Time-lapse images of septin localization in WT cells during RTG (A) and mitosis (B) and during RTG in the mutants (C). Numbers indicate time in minutes after initial recruitment of septins to the site of polarization. DIC, differential interference contrast. **(D)** Percentage of cells with abnormal septin localization in the bud during RTG and mitosis (n = 100 each). **(E)** Superresolution images showing the organization of bud-neck septin structures during RTG. Examples shown are observable defects, with each mutant having a range of defects. Bars: (A–C) 3 µm; (E) 1 µm. **(F)** Percentage of cells with defective bud-neck septin structures during RTG and mitosis from superresolution imaging (n = 50 each). **(D and F)** Differences between RTG and mitosis are statistically significant (Two-tailed Fisher's exact test; $P < 0.05$) unless marked ns.

Overall, these results suggest a model in which an extended G2/M delay with continued apical bud growth leads to prolonged local accumulation of GTP-Cdc42 that recruits septins to the bud tip, producing elongated buds with multiple septin structures. As GTP-Cdc42 and the septins localized to the bud tip, the septin collar at the bud neck was disrupted. Our data demonstrate that a prolonged G2/M checkpoint can be disruptive to the cell, causing defects in cell morphogenesis, spindle positioning, and septin organization.

Discussion

This study analyzed an alternative developmental program in budding yeast called RTG to determine how cells establish polarity and bud from a different cell cycle stage than in a normal mitosis. We focused on cells that enter mitosis from meiotic prophase I because this transition provides a fascinating case study of cell cycle regulation associated with major morphogenetic changes. Cells in prophase I are undergoing meiosis-specific events and lack polarized growth. When the cells reenter mitosis, they establish polarity and initiate budding from G2. Therefore, the cells bud after DNA replication but before nuclear division. This order of events is in contrast with that of normal mitosis in which cells establish polarity and form a bud in G1 before DNA replication (Howell and Lew, 2012).

We found that during RTG, cells ensure normal morphogenesis through careful regulation of CDK activity by the Swe1 kinase, which phosphorylates and inhibits CDK, and the Mih1 phosphatase, which removes the inhibitory phosphorylation (Russell et al., 1989; Booher et al., 1993). Premature M-CDK activity during RTG in *swe1Δ* cells results in a failure to polarize and bud before nuclear division, causing binucleate polyploid cells (Fig. 2;

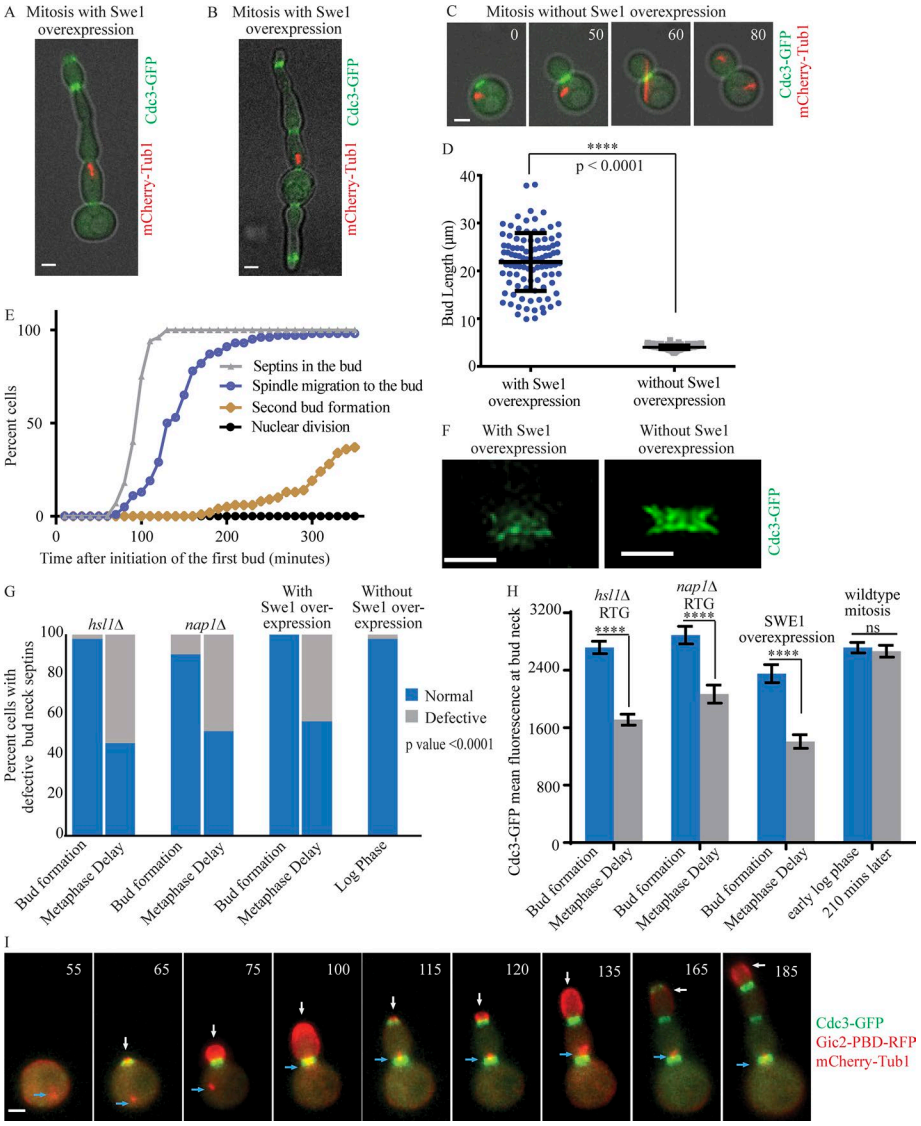

Figure 7. **Prolonged Swe1 overexpression causes elongated buds, multiple buds, spindle mispositioning, and septin defects during mitosis. (A and B)** Image showing an elongated bud, aberrant spindle position, and septin localized in the bud after Swe1 overexpression for 360 min. **(C)** Time-lapse images of a cell without Swe1 overexpression with time in minutes after initial recruitment of septins. **(D)** Mean bud length after 360 min of Swe1 overexpression or without Swe1 overexpression at the time of anaphase onset (error bars indicate SD; *n* = 100 each). **(E)** Septin localization in the bud, spindle migration to the bud, second bud formation, and nuclear division in WT cells overexpressing Swe1 (*n* = 100). **(F)** Superresolution images of bud-neck septin structures with Swe1 overexpression for 360 min or without Swe1 overexpression at anaphase onset. **(G)** Percentage of cells with defective versus normal bud-neck septin structures analyzed by superresolution imaging at individual time points. Septins were imaged at early bud formation and at metaphase delay (400 min after nutrient addition for *hsl1Δ* and *nap1Δ*; 360 min after *SWE1* induction; *n* = 50 each). Septins in a culture without Swe1 overexpression were imaged at log phase (*n* = 50 each). Differences are statistically significant (Two-tailed Fisher's exact test; P < 0.0001). **(H)** Mean fluorescence intensity of Cdc3-GFP at the bud neck measured at bud formation and at a metaphase delay (210 min later) for *hsl1Δ*, *nap1Δ*, and Swe1 overexpression (error bars indicate SEM). WT control cells were imaged in early log phase and 210 min later (*n* = 30 each). **(D and H)** Differences were statistically significant (Mann-Whitney test with computation of two-tailed exact p-value; ****, P < 0.0001) unless marked ns. **(I)** Time-lapse images of persistent GTP-Cdc42 localization at the bud tip and subsequent recruitment of septins in a cell overexpressing Swe1 during mitosis with time in minutes after galactose induction. White arrows indicate Gic2-PDB-RFP localization; blue arrows indicate mCherry-Tub1. Bars: (A–C and I) 3 µm; (F) 1 µm.

Tsuchiya and Lacefield, 2013). However, prolonged M-CDK inhibition during RTG in *mih1Δ* cells results in abnormally long buds. These phenotypes are characteristics of RTG; they do not occur in *swe1Δ* and *mih1Δ* cells during a normal mitosis (Fig. 2; Russell et al., 1989; Booher et al., 1993). Therefore, in RTG, Swe1 and Mih1 have essential roles in regulating the duration of G2/M to establish cell polarity and for normal morphogenesis, respectively.

Prolonged Swe1 activity causes exacerbated morphological defects and abnormal nuclear migration in RTG compared with mitosis

Our genetic screen uncovered eight PGRs that affected cell morphology during RTG. The mutants also had novel and more penetrant phenotypes during RTG when compared with mitosis. Seven mutants had enhanced elongated buds during RTG when compared with mitosis: *mih1Δ*, *clb2Δ*, *hsl7Δ*, *hsl1Δ*, *gin4Δ*, *nap1Δ*, and *cla4Δ* (Fig. 3). Additionally, one mutant, *elm1Δ*, had elongated buds in both mitosis and RTG but displayed more spindle positioning defects in RTG (Figs. 3 and 5). *hsl1Δ*, *gin4Δ*, and *nap1Δ* also had spindle position defects, which could be caused by defective bud neck septin structures. Previous work has shown that microtubules interact with the bud neck and that septins and septin-regulatory kinases ensure proper spindle positioning and nuclear migration (Kusch et al., 2002). The *hsl1Δ*, *gin4Δ*, *nap1Δ*, and *cla4Δ* cells produced multiple elongated buds from the mother cell before dividing, a rare phenotype in mitosis (Fig. 4). The *cla4Δ* mutants failed to divide during the duration of the experiment, suggesting that Cla4 is essential for RTG. The enhanced severity of this phenotype when compared with the other mutants can be explained by the fact that Cla4 is an upstream regulator of septin assembly and of some of the septin-regulating genes such as Gin4 (Mortensen et al., 2002;

Dobbelaere et al., 2003; Gladfelter et al., 2004; Kadota et al., 2004; Sakchaisri et al., 2004; Versele and Thorner, 2004). Cla4 also has a role in Swe1 inactivation (Sakchaisri et al., 2004).

Sustained morphogenesis checkpoint activity in mitosis causes perturbed septin structures

Why are there additional and exacerbated morphogenesis defects during RTG compared with mitosis? Our data show that this is likely caused by enhanced Swe1 activity. During RTG, perturbations that led to lower M-CDK activity (*clb2Δ* and *mih1Δ*) or enhanced Swe1 activity because of septin disruption or Swe1 inactivation (*hsl7Δ*, *hsl1Δ*, *gin4Δ*, *nap1Δ*, *elm1Δ*, and *cla4Δ*) led to protracted Swe1-dependent M-CDK down-regulation (Figs. 3 and 4). Previous work from Gladfelter et al. (2005) showed that minor perturbations in septin organization could be exacerbated by prolonged Swe1 activity. Therefore, in the *gin4Δ*, *nap1Δ*, *elm1Δ*, and *cla4Δ* mutants, defects in septins could be exacerbated during RTG because of prolonged Swe1 activity.

In addition, our results demonstrate that prolonged Swe1 activity alone, without underlying septin defects, is sufficient to perturb septin organization and localization. Mutants including *clb2Δ*, *mih1Δ*, and *hsl7Δ*, which have no known roles in septin organization, also had septin defects during RTG (Fig. 6). We hypothesized that if a prolonged G2/M delay could cause the disruption of septin structures and additional septin structures in RTG, the delay could also cause these defects in mitosis. To test this hypothesis, we overexpressed Swe1 in mitotic cells and examined septin collars with time-lapse imaging and superresolution microscopy. Indeed, we found that prolonged G2/M delay led to additional septin structures in the elongated bud and disrupted bud neck septin collars (Fig. 7). Furthermore, GTP-Cdc42 was localized at the tip of the elongated buds.

From our results, we conclude that a lengthy delay at G2/M perturbs septin organization. This result was unexpected because checkpoints normally delay the cell cycle to allow additional time to correct errors, whereas prolonged morphogenesis checkpoint activity resulted in septin perturbation. Furthermore, the formation of additional septin structures and continued polarized growth could suggest that the cells are in a process of rebudding without undergoing cell division. The continuation of cell cycle events without the completion of other events is counter to the classical definition of a checkpoint in which control mechanisms establish dependencies on the completion of other cell cycle events (Hartwell and Weinert, 1989).

Our data support the model of a feedback loop in which a G2/M delay causes septin defects, which further delays G2/M because the septin defects lead to increased Swe1 activity. Our results demonstrate that a Swe1-dependent delay causes elongated buds with prolonged localization of GTP-Cdc42 at the bud tip. Because GTP-Cdc42 recruits septins at the cortical bud site, we propose that with increased Swe1 activity, GTP-Cdc42 recruits the septins ectopically to the bud tip. This is supported by the time-lapse imaging of WT cells overexpressing *SWE1* in mitosis in which we saw Cdc3-GFP localize to the GTP-Cdc42 biosensor accumulated at the bud tip (Fig. 7 I and Video 6). Furthermore, the G2/M delay also led to the disruption of septin organization at the bud neck, with dimmer and disorganized structures over time (Fig. 7, F–H). Thus, the disruption of the septins could feed back to prolong Swe1 activity. This in turn would lead to an extended G2/M delay and further exacerbate the defects. In conclusion, our results reveal that prolonged activation of a G2/M checkpoint can be detrimental to the cell instead of beneficial.

Materials and methods

Strains and manipulations

Strains used in this study are derivatives of W303 (listed in Table S2). *SWE1* promotor swaps and gene deletions were made using standard PCR-based transformation methods (Longtine et al., 1998b; Janke et al., 2004; Sheff and Thorn, 2004). For gene deletions, we amplified the KanMX deletion cassette using short oligonucleotides that annealed upstream and downstream of the target gene from genomic DNA of mutant strains from the yeast knockout collection (Tong et al., 2001). To delete *HSL7*, we amplified the HphMX deletion cassette using oligonucleotides that harbored homology sequences flanking the *HSL7* ORF. To swap the *SWE1* promotor with the *GAL1* promotor, we amplified the *GAL1* promotor sequence from a plasmid (pYM-N23) with oligonucleotides that harbored homology sequences to target the PCR product at the *SWE1* promotor locus. Manipulation was confirmed by PCR. To tag ZIP1 with GFP, a plasmid (pHW122) carrying ZIP1-GFP:URA3 was linearized with HpaI and integrated into the *ZIP1* locus (plasmid provided by D. Kaback, Rutgers New Jersey Medical School, Newark, NJ; Scherthan et al., 2007). The *URA3* was looped out and selected for on 5FOA. Plasmids containing *GFP-TUB1* (pAFS125 linearized with StuI, provided by A. Murray, Harvard University, Cambridge, MA), *mCherry-TUB1* (pLB74 linearized with XbaI), *GIC2-PBD-RFP* (YIp211-GIC2PBD(W23A)-RFP linearized with ApaI, provided by E. Bi, University of Pennsylvania, Philadelphia, PA), and *CDC3-GFP* (YIp128-CDC3-GFP linearized with BglII, provided by E. Bi) were integrated into the genome at ura3, *TUB1*, *ura3*, and *leu2*, respectively. Insertions were confirmed by fluorescence microscopy.

Oligonucleotide sequences

For gene deletion (forward and reverse), we used: *NDT80*, 5′-CTTGGAGGGCAAAGTGTCAG-3′ and 5′-CAGCAGTGTCAAGCCAAATGC-3′; *MIH1*, 5′-AGAGCAGTGGACAAACCAGG-3′ and 5′-GATGTTGTTGCCGTTCGGTTC-3′; *SWE1*, 5′-GTCTTCCATCCTTCCCTT-3′ and 5′-GAACATTGGCGTGCCCC-3′; *CLB2*, 5′-TGAAGCGGTTCTTTGATTGAGC-3′ and 5′-GTCTACCCTCGCTACATGCA-3′; *HSL7*, 5′-TTTTATACATATAATTTTTATATATACAAAGGGTTCAGTTTGCATCGTACGCTGCAGGTCGAC-3′ and 5′-TGGATAGTTATTTGTTGCCGCAGTATATAGTATACAATGCAGAATATCGATGAATTCGAGCTCG-3′; *HSL1*, 5′-AACGACATAGATTTGCGGGAC-3′ and 5′-CTTTCCTTCGTGTCTCATGTCTC-3′; *GIN4*, 5′-CGCGAAATATCAACGGCCAC-3′ and 5′-CTTCTTGTCGGCCTCATTGTTCAT-3′; *NAP1*, 5′-ACAAGTTGGTGGGAAATGAGC-3′ and 5′-GTCGTCTTAGTTACATGCGCTT-3′; *ELM1*, 5′-ACAATGCAACAGTCTCTAGTCC-3′ and 5′-GCTAACCCAATCCGACAGATAT-3′; and *CLA4*, 5′-ATTCCTGGTGGTTTCTTTGGTG-3′ and 5′-GAAGCTGAAGCATGGACGAATA-3′.

For SWE1 promotor swap (forward and reverse), we used: 5′-CGCTCACGATGACCTGCAGGATTTTTCTCTTCTTTAACCTAATCAGCATTCGTACGCTGCAGGTCGAC-3′ and 5′-TCCGTGTCCAGC

ATTTCGAAGTCCTCTTCATCCTCGTCCAAAGAACTCATCGAT GAATTCTCTGTCG-3′.

Screen

The screen was performed as described in Fig. S1.

Growth conditions

For RTG experiments, cells were grown to saturation in YPD (1% bacto–yeast extract, 2% bactopeptone, and 2% glucose) at 30°C, transferred to YPA (1% yeast extract, 2% bactopeptone, and 1% potassium acetate) for 12–16 h at 30°C, and then incubated at 25°C in 1% potassium acetate for 10–12 h. They were then induced to return to mitosis by transfer to Synthetic Complete (SC) medium (0.67% bacto–yeast nitrogen base without amino acids, 0.2% dropout mix with all amino acids, and 2% glucose; Tsuchiya and Lacefield, 2013). For mitosis experiments, cells were grown in YPD or SC medium. To overexpress *SWE1*, cells with *GAL1* promoted *SWE1*, were grown in raffinose overnight, and then were transferred to SC galactose medium (2% galactose). For budding pattern experiments, cells were grown in SC medium with 0.5 µg/ml of calcofluor (Sigma-Aldrich).

Microscope image acquisition, time-lapse microscopy, fluorescence measurement, and image processing

Four microscope systems were used for this study. During the primary screen, cells were fixed with 4% paraformaldehyde, stained with DAPI, resuspended in PBS, and imaged at room temperature using a Pathway 855 BioImager (BD) equipped with an ORCA charge-coupled device camera and a 60× oil objective (Plan Apochromat-N, 1.4 NA; Hamamatsu Photonics). The exposure time was 10–100 ms. During the secondary screen, cells were loaded on a coverslip and under an agar pad containing SC medium; they were then imaged at room temperature in RTG and in mitosis with a DeltaVision pDV microscope (Applied Precision, Ltd.) equipped with a CoolSNAP HQ2/HQ2-ICX285 camera using a 60× oil objective (U-Plan S-Apochromat-N, 1.4 NA). The cells harbored an mCherry or a GFP tag fused to the *TUB1* gene to visualize the spindle or an RFP tag fused to Gic2-PBD to visualize active Cdc42. A GFP tag was also added to the *ZIP1* gene to visualize the synaptonemal complex and to the *CDC3* gene to visualize septins (See the Strains and manipulations section). Images were acquired using SoftWoRx software (GE Healthcare).

During time-lapse imaging on DeltaVision, five z steps (0.8 µm) were acquired every 10 min for 8–10 h in RTG and for 6 h in mitosis. The exposure time was 200–500 ms with neutral density filters transmitting 2–32% of light intensity. Calcofluor-stained cells were also imaged at room temperature with the DeltaVision in liquid SC medium in a chamber mounted on a coverslip coated with Concanavalin A (Sigma-Aldrich). Cells overexpressing *SWE1* in mitosis were imaged live at 25°C with a T*i*-E inverted-objective microscope (Nikon) equipped with CoolSNAP HQ2 charge-coupled device camera and a 60× oil objective (Plan Apochromat VC, 1.4 NA) using an ONIX microfluidics system (EMD Millipore). Control cells were imaged in SC medium with 2% raffinose, and cells overexpressing *SWE1* were imaged in SC medium with 2% galactose. Images were acquired with NIS Elements AR software (Nikon). Five z steps (1.2 µm) were acquired every 10 min for 7 h. The exposure time was 500–800 ms with 8–16 neutral-density filters. Maximum-intensity projections were performed to obtain the final images presented in this article.

Structural illumination microscopy (OMX 3D-SIM superresolution system; GE Healthcare) was used to image bud-neck septin structures of cells growing in SC medium. Cells were loaded (without fixation) under an agar pad containing SC medium on a slide coated with Concanavalin A, and they were imaged at room temperature using a 100× oil objective (U-Plan S-Apochromat, 1.4 NA). Images were acquired by the DeltaVision OMX software using a Photometrics Cascade II electron-multiplying charge-coupled device camera. Raw images were reconstructed using the OMX SI Reconstruction tool in SoftWoRx.

All images were processed using ImageJ (National Institutes of Health). Fluorescence images presented in this study show maximum projections from multiple z series. Brightness and contrast were adjusted on entire images to balance multiple fluorescence colors. To measure Cdc3-GFP fluorescence intensity, cells were taken from SC culture tubes at different time points and mounted (without fixation) on a coverslip under an agar pad also containing SC medium. Images were then acquired on the pDV DeltaVision microscope with a 40× objective (U-Plan Apochromat, 0.9 NA; Olympus). Three z sections were taken for each image, and fluorescence intensity was measured from a sum of the z sections using ImageJ.

To assess the budding pattern, ImageJ software was used to measure the budding angle. A fit circle was drawn along the cell's circumference. The line tool was then used to draw a square with four corner points on the fit circle. Two diameters of the fit circle were drawn such that they pass through the corner points of the square and so intersect at center of the fit circle. The diameter intersection point was considered the approximate center of the cell. The angle tool was then used to measure the central angle between the previous and the nascent division sites, which were marked with calcofluor. To measure the bud lengths, the ImageJ line tool was used to draw a straight line from the bud neck to the bud tip. The measure of the length of this line was taken as the approximate length of the bud.

Western blots

After transferring the cells to SC medium to induce RTG, protein extraction was performed every 30 min for a total of 300 min. Harvested cells were vortexed vigorously (6 × 30–s vortex followed by 30 s incubation on ice) in the presence of 0.1-mm glass beads in PME (0.1 M Pipes, 0.001 M $MgSO_4$, and 0.002 M EGTA) and buffer at 4°C. Protease inhibitors (Roche) were added to the PME buffer before mixing with the cells. The extracts were then boiled for 5 min at 96°C in GSD (30% glycerol, 6.6% sodium dodecyl sulfate, and 0.05% DTT) sample buffer. Boiled extracts were centrifuged for 2 min at 14,000 rpm, and proteins were collected in the supernatant and stored at −80°C. Western blot analysis was performed using a rabbit anti-Cdc2 phosphotyrosine (1:1,000; AB3241-25UL; EMD Millipore) and a mouse anti–phosphoglycerate kinase 1 (PGK1; 1:10,000; 459250; Novex Life Technologies). The secondary antibodies were goat anti–rabbit (1:3,000) and goat anti–mouse (1:5,000) IgG ECL antibodies linked to HRP (GE Healthcare). Three

independent replicate experiments were performed, and the band signal intensity was measured using ImageJ.

Statistical analysis

All statistical analyses were performed using Prism (GraphPad Software). Statistical analysis of the timing of GTP-Cdc42 accumulation, bud formation, and anaphase onset as well as of bud length and fluorescence intensity was done using an unpaired, nonparametric Mann-Whitney test with computation of two-tailed exact p-values. Compared data were entered into grouped-format tables with individual data values entered into subcolumns. The number of data points (n) is indicated in the figure legends. To analyze the data presented as percentages, we used the two-sided Fisher's exact test. Individual percentages were computed into Excel spreadsheets (Microsoft) and entered into Prism contingency tables. The number of cells analyzed in every experiment is indicated in the figure legends. Difference among compared data was considered statistically significant if the p-value was <0.05.

Online supplemental material

Fig. S1 shows bud site selection and detailed screen design. Fig. S2 shows duplicates and quantification of Western blots, showing enhanced M-CDK phosphorylation in the mutant strains. Fig. S3 shows quantification of the spindle positioning defects observed during mitosis and RTG. Table S1 shows time of bud formation and anaphase onset in RTG and mitosis. Table S2 shows yeast strains used in this study. Video 1 shows multiple budding in a *cla4Δ* cell (GFP-Tub1, spindle). Video 2 shows septin-aberrant localization to the bud of an *elm1Δ* cell (Cdc3-GFP, septins; mCherry-Tub1, spindle). Video 3 shows septin- and spindle-aberrant localization to the bud of a cell overexpressing *SWE1* (Cdc3-GFP, septins; mCherry-Tub1, spindle). Video 4 shows normal septin localization at the bud neck in a WT cell (Cdc3-GFP, septins; mCherry-Tub1, spindle). Video 5 shows multiple buds and aberrant septin localization in a cell overexpressing *SWE1* (Cdc3-GFP, septins; mCherry-Tub1, spindle). Video 6 shows septins following active Cdc42 at the tip of an elongating bud of a cell overexpressing *SWE1* (Cdc3-GFP, septins; mCherry-Tub1, spindle; Gic2-PBD-RFP, active Cdc42).

Acknowledgments

We are grateful to Andrew Murray and Erfei Bi for strains and constructs. We thank Sid Shaw, Jim Powers, and the Indiana University Light Microscopy and Imaging Center for imaging support. We thank Frank Solomon for comments. We thank Justin Kumar and Irene Newton for use of equipment.

This work was supported by the National Institutes of Health (GM105755).

The authors declare no competing financial interests.

Author contributions: G.M. Gihana and S. Lacefield designed and performed experiments and analyzed the data. T.R. Musser and O. Thompson created critical strains used in the study. S. Lacefield supervised and acquired funding for the project. G.M. Gihana and S. Lacefield wrote the manuscript with input from all authors.

Submitted: 23 August 2017
Revised: 1 March 2018
Accepted: 16 April 2018

References

Adams, A.E., D.I. Johnson, R.M. Longnecker, B.F. Sloat, and J.R. Pringle. 1990. CDC42 and CDC43, two additional genes involved in budding and the establishment of cell polarity in the yeast Saccharomyces cerevisiae. *J. Cell Biol.* 111:131–142. https://doi.org/10.1083/jcb.111.1.131

Alexander, M.R., M. Tyers, M. Perret, B.M. Craig, K.S. Fang, and M.C. Gustin. 2001. Regulation of cell cycle progression by Swe1p and Hog1p following hypertonic stress. *Mol. Biol. Cell.* 12:53–62. https://doi.org/10.1091/mbc.12.1.53

Altman, R., and D. Kellogg. 1997. Control of mitotic events by Nap1 and the Gin4 kinase. *J. Cell Biol.* 138:119–130. https://doi.org/10.1083/jcb.138.1.119

Anastasia, S.D., D.L. Nguyen, V. Thai, M. Meloy, T. MacDonough, and D.R. Kellogg. 2012. A link between mitotic entry and membrane growth suggests a novel model for cell size control. *J. Cell Biol.* 197:89–104. https://doi.org/10.1083/jcb.201108108

Asano, S., J.E. Park, L.R. Yu, M. Zhou, K. Sakchaisri, C.J. Park, Y.H. Kang, J. Thorner, T.D. Veenstra, and K.S. Lee. 2006. Direct phosphorylation and activation of a Nim1-related kinase Gin4 by Elm1 in budding yeast. *J. Biol. Chem.* 281:27090–27098. https://doi.org/10.1074/jbc.M601483200

Barral, Y., M. Parra, S. Bidlingmaier, and M. Snyder. 1999. Nim1-related kinases coordinate cell cycle progression with the organization of the peripheral cytoskeleton in yeast. *Genes Dev.* 13:176–187. https://doi.org/10.1101/gad.13.2.176

Bi, E., and H.O. Park. 2012. Cell polarization and cytokinesis in budding yeast. *Genetics.* 191:347–387. https://doi.org/10.1534/genetics.111.132886

Blacketer, M.J., C.M. Koehler, S.G. Coats, A.M. Myers, and P. Madaule. 1993. Regulation of dimorphism in Saccharomyces cerevisiae: involvement of the novel protein kinase homolog Elm1p and protein phosphatase 2A. *Mol. Cell. Biol.* 13:5567–5581. https://doi.org/10.1128/MCB.13.9.5567

Booher, R.N., R.J. Deshaies, and M.W. Kirschner. 1993. Properties of Saccharomyces cerevisiae wee1 and its differential regulation of p34CDC28 in response to G1 and G2 cyclins. *EMBO J.* 12:3417–3426.

Bouquin, N., Y. Barral, R. Courbeyrette, M. Blondel, M. Snyder, and C. Mann. 2000. Regulation of cytokinesis by the Elm1 protein kinase in Saccharomyces cerevisiae. *J. Cell Sci.* 113:1435–1445.

Chant, J., and J.R. Pringle. 1995. Patterns of bud-site selection in the yeast Saccharomyces cerevisiae. *J. Cell Biol.* 129:751–765. https://doi.org/10.1083/jcb.129.3.751

Cid, V.J., M.J. Shulewitz, K.L. McDonald, and J. Thorner. 2001. Dynamic localization of the Swe1 regulator Hsl7 during the Saccharomyces cerevisiae cell cycle. *Mol. Biol. Cell.* 12:1645–1669. https://doi.org/10.1091/mbc.12.6.1645

Cvrcková, F., C. De Virgilio, E. Manser, J.R. Pringle, and K. Nasmyth. 1995. Ste20-like protein kinases are required for normal localization of cell growth and for cytokinesis in budding yeast. *Genes Dev.* 9:1817–1830. https://doi.org/10.1101/gad.9.15.1817

Dayani, Y., G. Simchen, and M. Lichten. 2011. Meiotic recombination intermediates are resolved with minimal crossover formation during return-to-growth, an analogue of the mitotic cell cycle. *PLoS Genet.* 7:e1002083. https://doi.org/10.1371/journal.pgen.1002083

Dobbelaere, J., M.S. Gentry, R.L. Hallberg, and Y. Barral. 2003. Phosphorylation-dependent regulation of septin dynamics during the cell cycle. *Dev. Cell.* 4:345–357. https://doi.org/10.1016/S1534-5807(03)00061-3

Enserink, J.M., and R.D. Kolodner. 2010. An overview of Cdk1-controlled targets and processes. *Cell Div.* 5:11. https://doi.org/10.1186/1747-1028-5-11

Esposito, R.E., and M.S. Esposito. 1974. Genetic recombination and commitment to meiosis in Saccharomyces. *Proc. Natl. Acad. Sci. USA.* 71:3172–3176. https://doi.org/10.1073/pnas.71.8.3172

Farkas, V., J. Kovarík, A. Kosinová, and S. Bauer. 1974. Autoradiographic study of mannan incorporation into the growing cell walls of Saccharomyces cerevisiae. *J. Bacteriol.* 117:265–269.

Freifelder, D. 1960. Bud position in Saccharomyces cerevisiae. *J. Bacteriol.* 80:567–568.

Friedlander, G., D. Joseph-Strauss, M. Carmi, D. Zenvirth, G. Simchen, and N. Barkai. 2006. Modulation of the transcription regulatory program in yeast cells committed to sporulation. *Genome Biol.* 7:R20. https://doi.org/10.1186/gb-2006-7-3-r20

Ganesan, A.T., H. Holter, and C. Roberts. 1958. Some observations on sporulation in Saccharomyces. *C.R. Trav. Lab. Carlsberg Chim.* 31:1–6.

Gladfelter, A.S., T.R. Zyla, and D.J. Lew. 2004. Genetic interactions among regulators of septin organization. *Eukaryot. Cell.* 3:847–854. https://doi.org/10.1128/EC.3.4.847-854.2004

Gladfelter, A.S., L. Kozubowski, T.R. Zyla, and D.J. Lew. 2005. Interplay between septin organization, cell cycle and cell shape in yeast. *J. Cell Sci.* 118:1617–1628. https://doi.org/10.1242/jcs.02286

Gould, K.L., and P. Nurse. 1989. Tyrosine phosphorylation of the fission yeast cdc2+ protein kinase regulates entry into mitosis. *Nature.* 342:39–45. https://doi.org/10.1038/342039a0

Gould, K.L., S. Moreno, N.K. Tonks, and P. Nurse. 1990. Complementation of the mitotic activator, p80cdc25, by a human protein-tyrosine phosphatase. *Science.* 250:1573–1576. https://doi.org/10.1126/science.1703321

Gulli, M.P., M. Jaquenoud, Y. Shimada, G. Niederhäuser, P. Wiget, and M. Peter. 2000. Phosphorylation of the Cdc42 exchange factor Cdc24 by the PAK-like kinase Cla4 may regulate polarized growth in yeast. *Mol. Cell.* 6:1155–1167. https://doi.org/10.1016/S1097-2765(00)00113-1

Harkins, H.A., N. Pagé, L.R. Schenkman, C. De Virgilio, S. Shaw, H. Bussey, and J.R. Pringle. 2001. Bud8p and Bud9p, proteins that may mark the sites for bipolar budding in yeast. *Mol. Biol. Cell.* 12:2497–2518. https://doi.org/10.1091/mbc.12.8.2497

Hartwell, L.H., and T.A. Weinert. 1989. Checkpoints: controls that ensure the order of cell cycle events. *Science.* 246:629–634. https://doi.org/10.1126/science.2683079

Harvey, S.L., and D.R. Kellogg. 2003. Conservation of mechanisms controlling entry into mitosis: budding yeast wee1 delays entry into mitosis and is required for cell size control. *Curr. Biol.* 13:264–275. https://doi.org/10.1016/S0960-9822(03)00049-6

Harvey, S.L., A. Charlet, W. Haas, S.P. Gygi, and D.R. Kellogg. 2005. Cdk1-dependent regulation of the mitotic inhibitor Wee1. *Cell.* 122:407–420. https://doi.org/10.1016/j.cell.2005.05.029

Honigberg, S.M., and R.E. Esposito. 1994. Reversal of cell determination in yeast meiosis: postcommitment arrest allows return to mitotic growth. *Proc. Natl. Acad. Sci. USA.* 91:6559–6563. https://doi.org/10.1073/pnas.91.14.6559

Howell, A.S., and D.J. Lew. 2012. Morphogenesis and the cell cycle. *Genetics.* 190:51–77. https://doi.org/10.1534/genetics.111.128314

Janke, C., M.M. Magiera, N. Rathfelder, C. Taxis, S. Reber, H. Maekawa, A. Moreno-Borchart, G. Doenges, E. Schwob, E. Schiebel, and M. Knop. 2004. A versatile toolbox for PCR-based tagging of yeast genes: new fluorescent proteins, more markers and promoter substitution cassettes. *Yeast.* 21:947–962. https://doi.org/10.1002/yea.1142

Johnson, D.I., and J.R. Pringle. 1990. Molecular characterization of CDC42, a Saccharomyces cerevisiae gene involved in the development of cell polarity. *J. Cell Biol.* 111:143–152. https://doi.org/10.1083/jcb.111.1.143

Jorgensen, P., J.L. Nishikawa, B.J. Breitkreutz, and M. Tyers. 2002. Systematic identification of pathways that couple cell growth and division in yeast. *Science.* 297:395–400. https://doi.org/10.1126/science.1070850

Kadota, J., T. Yamamoto, S. Yoshiuchi, E. Bi, and K. Tanaka. 2004. Septin ring assembly requires concerted action of polarisome components, a PAK kinase Cla4p, and the actin cytoskeleton in Saccharomyces cerevisiae. *Mol. Biol. Cell.* 15:5329–5345. https://doi.org/10.1091/mbc.E04-03-0254

Kaiser, P., R.A. Sia, E.G. Bardes, D.J. Lew, and S.I. Reed. 1998. Cdc34 and the F-box protein Met30 are required for degradation of the Cdk-inhibitory kinase Swe1. *Genes Dev.* 12:2587–2597. https://doi.org/10.1101/gad.12.16.2587

Kang, H., D. Tsygankov, and D.J. Lew. 2016. Sensing a bud in the yeast morphogenesis checkpoint: a role for Elm1. *Mol. Biol. Cell.* 27:1764–1775. https://doi.org/10.1091/mbc.e16-01-0014

Kellogg, D.R., and A.W. Murray. 1995. NAP1 acts with Clb1 to perform mitotic functions and to suppress polar bud growth in budding yeast. *J. Cell Biol.* 130:675–685. https://doi.org/10.1083/jcb.130.3.675

Kennedy, E.K., M. Dysart, N. Lianga, E.C. Williams, S. Pilon, C. Doré, J.S. Deneault, and A.D. Rudner. 2016. Redundant Regulation of Cdk1 Tyrosine Dephosphorylation in Saccharomyces cerevisiae. *Genetics.* 202:903–910. https://doi.org/10.1534/genetics.115.182469

Kusch, J., A. Meyer, M.P. Snyder, and Y. Barral. 2002. Microtubule capture by the cleavage apparatus is required for proper spindle positioning in yeast. *Genes Dev.* 16:1627–1639. https://doi.org/10.1101/gad.222602

Lew, D.J., and S.I. Reed. 1993. Morphogenesis in the yeast cell cycle: regulation by Cdc28 and cyclins. *J. Cell Biol.* 120:1305–1320. https://doi.org/10.1083/jcb.120.6.1305

Lew, D.J., and S.I. Reed. 1995. A cell cycle checkpoint monitors cell morphogenesis in budding yeast. *J. Cell Biol.* 129:739–749. https://doi.org/10.1083/jcb.129.3.739

Lianga, N., E.C. Williams, E.K. Kennedy, C. Doré, S. Pilon, S.L. Girard, J.S. Deneault, and A.D. Rudner. 2013. A Wee1 checkpoint inhibits anaphase onset. *J. Cell Biol.* 201:843–862. https://doi.org/10.1083/jcb.201212038

Lim, H.H., P.Y. Goh, and U. Surana. 1996. Spindle pole body separation in Saccharomyces cerevisiae requires dephosphorylation of the tyrosine 19 residue of Cdc28. *Mol. Cell. Biol.* 16:6385–6397. https://doi.org/10.1128/MCB.16.11.6385

Longtine, M.S., H. Fares, and J.R. Pringle. 1998a. Role of the yeast Gin4p protein kinase in septin assembly and the relationship between septin assembly and septin function. *J. Cell Biol.* 143:719–736. https://doi.org/10.1083/jcb.143.3.719

Longtine, M.S., A. McKenzie III, D.J. Demarini, N.G. Shah, A. Wach, A. Brachat, P. Philippsen, and J.R. Pringle. 1998b. Additional modules for versatile and economical PCR-based gene deletion and modification in Saccharomyces cerevisiae. *Yeast.* 14:953–961. https://doi.org/10.1002/(SICI)1097-0061(199807)14:10%3C953::AID-YEA293%3E3.0.CO;2-U

Longtine, M.S., C.L. Theesfeld, J.N. McMillan, E. Weaver, J.R. Pringle, and D.J. Lew. 2000. Septin-dependent assembly of a cell cycle-regulatory module in Saccharomyces cerevisiae. *Mol. Cell. Biol.* 20:4049–4061. https://doi.org/10.1128/MCB.20.11.4049-4061.2000

Ma, X.J., Q. Lu, and M. Grunstein. 1996. A search for proteins that interact genetically with histone H3 and H4 amino termini uncovers novel regulators of the Swe1 kinase in Saccharomyces cerevisiae. *Genes Dev.* 10:1327–1340. https://doi.org/10.1101/gad.10.11.1327

McMillan, J.N., R.A. Sia, and D.J. Lew. 1998. A morphogenesis checkpoint monitors the actin cytoskeleton in yeast. *J. Cell Biol.* 142:1487–1499. https://doi.org/10.1083/jcb.142.6.1487

McMillan, J.N., C.L. Theesfeld, J.C. Harrison, E.S. Bardes, and D.J. Lew. 2002. Determinants of Swe1p degradation in Saccharomyces cerevisiae. *Mol. Biol. Cell.* 13:3560–3575. https://doi.org/10.1091/mbc.E02-05-0283

McNulty, J.J., and D.J. Lew. 2005. Swe1p responds to cytoskeletal perturbation, not bud size, in S. cerevisiae. *Curr. Biol.* 15:2190–2198. https://doi.org/10.1016/j.cub.2005.11.039

Mortensen, E.M., H. McDonald, J. Yates III, and D.R. Kellogg. 2002. Cell cycle-dependent assembly of a Gin4-septin complex. *Mol. Biol. Cell.* 13:2091–2105. https://doi.org/10.1091/mbc.01-10-0500

Nachman, I., A. Regev, and S. Ramanathan. 2007. Dissecting timing variability in yeast meiosis. *Cell.* 131:544–556. https://doi.org/10.1016/j.cell.2007.09.044

Okada, S., M. Leda, J. Hanna, N.S. Savage, E. Bi, and A.B. Goryachev. 2013. Daughter cell identity emerges from the interplay of Cdc42, septins, and exocytosis. *Dev. Cell.* 26:148–161. https://doi.org/10.1016/j.devcel.2013.06.015

Pal, G., M.T. Paraz, and D.R. Kellogg. 2008. Regulation of Mih1/Cdc25 by protein phosphatase 2A and casein kinase 1. *J. Cell Biol.* 180:931–945. https://doi.org/10.1083/jcb.200711014

Pringle, J.R. 1991. Staining of bud scars and other cell wall chitin with calcofluor. *Methods Enzymol.* 194:732–735. https://doi.org/10.1016/0076-6879(91)94055-H

Richman, T.J., M.M. Sawyer, and D.I. Johnson. 2002. Saccharomyces cerevisiae Cdc42p localizes to cellular membranes and clusters at sites of polarized growth. *Eukaryot. Cell.* 1:458–468. https://doi.org/10.1128/EC.1.3.458-468.2002

Russell, P., S. Moreno, and S.I. Reed. 1989. Conservation of mitotic controls in fission and budding yeasts. *Cell.* 57:295–303. https://doi.org/10.1016/0092-8674(89)90967-7

Sakchaisri, K., S. Asano, L.R. Yu, M.J. Shulewitz, C.J. Park, J.E. Park, Y.W. Cho, T.D. Veenstra, J. Thorner, and K.S. Lee. 2004. Coupling morphogenesis to mitotic entry. *Proc. Natl. Acad. Sci. USA.* 101:4124–4129. https://doi.org/10.1073/pnas.0400641101

Scherthan, H., H. Wang, C. Adelfalk, E.J. White, C. Cowan, W.Z. Cande, and D.B. Kaback. 2007. Chromosome mobility during meiotic prophase in Saccharomyces cerevisiae. *Proc. Natl. Acad. Sci. USA.* 104:16934–16939. https://doi.org/10.1073/pnas.0704860104

Sheff, M.A., and K.S. Thorn. 2004. Optimized cassettes for fluorescent protein tagging in Saccharomyces cerevisiae. *Yeast.* 21:661–670. https://doi.org/10.1002/yea.1130

Sherman, F., and H. Roman. 1963. Evidence for two types of allelic recombination in yeast. *Genetics.* 48:255–261.

Shulewitz, M.J., C.J. Inouye, and J. Thorner. 1999. Hsl7 localizes to a septin ring and serves as an adapter in a regulatory pathway that relieves tyrosine

phosphorylation of Cdc28 protein kinase in Saccharomyces cerevisiae. *Mol. Cell. Biol.* 19:7123–7137. https://doi.org/10.1128/MCB.19.10.7123

Sia, R.A., H.A. Herald, and D.J. Lew. 1996. Cdc28 tyrosine phosphorylation and the morphogenesis checkpoint in budding yeast. *Mol. Biol. Cell.* 7:1657–1666. https://doi.org/10.1091/mbc.7.11.1657

Sia, R.A., E.S. Bardes, and D.J. Lew. 1998. Control of Swe1p degradation by the morphogenesis checkpoint. *EMBO J.* 17:6678–6688. https://doi.org/10.1093/emboj/17.22.6678

Simchen, G., R. Piñon, and Y. Salts. 1972. Sporulation in Saccharomyces cerevisiae: premeiotic DNA synthesis, readiness and commitment. *Exp. Cell Res.* 75:207–218. https://doi.org/10.1016/0014-4827(72)90538-1

Sreenivasan, A., and D. Kellogg. 1999. The elm1 kinase functions in a mitotic signaling network in budding yeast. *Mol. Cell. Biol.* 19:7983–7994. https://doi.org/10.1128/MCB.19.12.7983

Straight, A.F., W.F. Marshall, J.W. Sedat, and A.W. Murray. 1997. Mitosis in living budding yeast: anaphase A but no metaphase plate. *Science.* 277:574–578. https://doi.org/10.1126/science.277.5325.574

Surana, U., H. Robitsch, C. Price, T. Schuster, I. Fitch, A.B. Futcher, and K. Nasmyth. 1991. The role of CDC28 and cyclins during mitosis in the budding yeast S. cerevisiae. *Cell.* 65:145–161. https://doi.org/10.1016/0092-8674(91)90416-V

Theesfeld, C.L., T.R. Zyla, E.G. Bardes, and D.J. Lew. 2003. A monitor for bud emergence in the yeast morphogenesis checkpoint. *Mol. Biol. Cell.* 14:3280–3291. https://doi.org/10.1091/mbc.E03-03-0154

Tong, A.H., M. Evangelista, A.B. Parsons, H. Xu, G.D. Bader, N. Pagé, M. Robinson, S. Raghibizadeh, C.W. Hogue, H. Bussey, et al. 2001. Systematic genetic analysis with ordered arrays of yeast deletion mutants. *Science.* 294:2364–2368. https://doi.org/10.1126/science.1065810

Tsuchiya, D., and S. Lacefield. 2013. Cdk1 modulation ensures the coordination of cell-cycle events during the switch from meiotic prophase to mitosis. *Curr. Biol.* 23:1505–1513. https://doi.org/10.1016/j.cub.2013.06.031

Tsuchiya, D., C. Gonzalez, and S. Lacefield. 2011. The spindle checkpoint protein Mad2 regulates APC/C activity during prometaphase and metaphase of meiosis I in Saccharomyces cerevisiae. *Mol. Biol. Cell.* 22:2848–2861. https://doi.org/10.1091/mbc.e11-04-0378

Tsuchiya, D., Y. Yang, and S. Lacefield. 2014. Positive feedback of NDT80 expression ensures irreversible meiotic commitment in budding yeast. *PLoS Genet.* 10:e1004398. https://doi.org/10.1371/journal.pgen.1004398

Uhlmann, F., C. Bouchoux, and S. López-Avilés. 2011. A quantitative model for cyclin-dependent kinase control of the cell cycle: revisited. *Philos. Trans. R. Soc. Lond. B Biol. Sci.* 366:3572–3583. https://doi.org/10.1098/rstb.2011.0082

Versele, M., and J. Thorner. 2004. Septin collar formation in budding yeast requires GTP binding and direct phosphorylation by the PAK, Cla4. *J. Cell Biol.* 164:701–715. https://doi.org/10.1083/jcb.200312070

Weiss, E.L., A.C. Bishop, K.M. Shokat, and D.G. Drubin. 2000. Chemical genetic analysis of the budding-yeast p21-activated kinase Cla4p. *Nat. Cell Biol.* 2:677–685. https://doi.org/10.1038/35036300

White, E.J., C. Cowan, W.Z. Cande, and D.B. Kaback. 2004. In vivo analysis of synaptonemal complex formation during yeast meiosis. *Genetics.* 167:51–63. https://doi.org/10.1534/genetics.167.1.51

Wicky, S., H. Tjandra, D. Schieltz, J. Yates III, and D.R. Kellogg. 2011. The Zds proteins control entry into mitosis and target protein phosphatase 2A to the Cdc25 phosphatase. *Mol. Biol. Cell.* 22:20–32. https://doi.org/10.1091/mbc.e10-06-0487

Winter, E. 2012. The Sum1/Ndt80 transcriptional switch and commitment to meiosis in Saccharomyces cerevisiae. *Microbiol. Mol. Biol. Rev.* 76:1–15. https://doi.org/10.1128/MMBR.05010-11

Xu, L., M. Ajimura, R. Padmore, C. Klein, and N. Kleckner. 1995. NDT80, a meiosis-specific gene required for exit from pachytene in Saccharomyces cerevisiae. *Mol. Cell. Biol.* 15:6572–6581. https://doi.org/10.1128/MCB.15.12.6572

Zenvirth, D., J. Loidl, S. Klein, A. Arbel, R. Shemesh, and G. Simchen. 1997. Switching yeast from meiosis to mitosis: double-strand break repair, recombination and synaptonemal complex. *Genes Cells.* 2:487–498. https://doi.org/10.1046/j.1365-2443.1997.1370335.x

Ziman, M., D. Preuss, J. Mulholland, J.M. O'Brien, D. Botstein, and D.I. Johnson. 1993. Subcellular localization of Cdc42p, a Saccharomyces cerevisiae GTP-binding protein involved in the control of cell polarity. *Mol. Biol. Cell.* 4:1307–1316. https://doi.org/10.1091/mbc.4.12.1307